IEEE Access
Multidisciplinary | Rapid Review | Open Access Journal

Received September 23, 2020, accepted October 5, 2020, date of publication October 8, 2020, date of current version October 21, 2020.

Digital Object Identifier 10.1109/ACCESS.2020.3029635

Path Tracking Control Based on Model Predictive Control With Adaptive Preview Characteristics and Speed-Assisted Constraint

CHANGHUA DAI[1], CHANGFU ZONG[2], AND GUOYING CHEN[2]
[1]College of Automotive Engineering, Jilin University, Changchun 130012, China
[2]State Key Laboratory of Automotive Simulation and Control, Jilin University, Changchun 130012, China

Corresponding author: Guoying Chen (cgy-011@163.com)

This work was supported in part by the National Natural Science Foundation of China under Grant 51575224 and Grant 51505178, and in part by the China Postdoctoral Science Foundation under Grant 2014M561289.

ABSTRACT As one of the research focuses in the field of intelligent driving, improving the performance of path tracking has become a goal for many scholars. Among many path tracking control algorithms, model predictive control (MPC) controllers are widely used due to their excellent control performance. However, the traditional MPC control has shortcomings because it does not consider the particularity of the driving car with preview driving characteristics, i.e., it is only directly controlling from the vehicle state. To fully retain the advantages of the MPC controller and simultaneously exert the preview characteristic of the intelligent vehicle to improve the path tracking performance, this work proposes a model predictive control with adaptive preview characteristics and an algorithm of longitudinal vehicle speed-assisted constraint for the path tracking algorithm. The algorithm mainly consists of two parts: The MPC controller with adaptive preview characteristic is proposed based on the lateral error and target curvature; The longitudinal vehicle speed-assisted constraint algorithm based on the largest ideal lateral acceleration becomes a supplementary part of the algorithm as a supplementary constraint of the MPC controller. Series of simulations based on the Simulink/CARSIM software individually verified the model predictive control with adaptive preview characteristics and an algorithm of longitudinal vehicle speed-assisted constraint for the path tracking algorithm. The proposed adaptive preview strategy is suitable for the path tracking algorithm controlled by the MPC controller and improves the path tracking performance.

INDEX TERMS Path tracking, model predictive control (MPC), adaptive preview characteristics, assisted constraint.

I. INTRODUCTION

At present, intelligent driving technology is mainly divided into environment perception and localization, decision planning and tracking control [1]–[3]. Among them, as the underlying technology of intelligent driving, path tracking has a more direct impact on intelligent driving effects [4] than environmental awareness and decision planning. If the performance of various indicators of the path tracking can be greatly improved, the level of intelligent driving is improved, which is a great significance to enterprises and countries. Therefore, many scholars currently conduct in-depth research to improve the performance of various indicators of path tracking [5]–[11]. The algorithms currently applied in path tracking control are mainly divided into six categories: geometric and kinematic algorithms, dynamic algorithms, optimal algorithms, adaptive algorithms, model-based algorithms and classical algorithms [3]. These studies can be divided into two major directions. One direction is directly from the perspective of vehicle status to control, which is learned from robot control problems, such as optimal algorithms, adaptive algorithms, model-based algorithms and classical algorithms. The other direction is to propose a control method from the perspective of a comprehensive consideration of the vehicle characteristics and driver characteristics, such as geometric and kinematic algorithms and dynamic algorithms, which consider the preview characteristics of the driver.

Path tracking control can be considered an automatic execution system that replaces the real driver, which should have the driving characteristics of a real driver [12], [13]. The most

The associate editor coordinating the review of this manuscript and approving it for publication was Nishant Unnikrishnan.

remarkable driving characteristic of a driver is the preview process, where the driver selects a point on the path at a distance from the front of the vehicle as a driving reference point. The preview optimal curvature control described in [14] is this idea. The tracking control of the intelligent vehicle is different from the tracking control problem of the robot. The preview operation is the main characteristic and strategy of the intelligent vehicle path tracking control.

Among the mentioned algorithms, because of their significant advantages for complex coupled systems, multiple inputs and multiple outputs, multiconstraint control issues [15]–[17] and predictive capabilities [18], model predictive controllers have been the research hotspot in the field of path tracking control of intelligent vehicles. In particular, in recent years, the performance of portable supercomputers that can handle complex algorithms and computing power requirements has been increasing [3], which enables this type of control method in the intelligent vehicle field. Many studies have been conducted, e.g., [19] presents a linear model predictive control approach to design a moving horizon path tracking controller to solve the situations that may cause collision and run-out-of-road issues in the traditional path tracking method. Reference [20] proposes a linear model-based MPC path-tracking steering controller for autonomous vehicles. [21], [22] propose model predicted control algorithms to solve the path-tracking problem of terrestrial autonomous vehicles. In [23], a path-tracking controller formulated the tracking task as a multiconstrained model predictive control problem and calculated the front steering angle to prevent the vehicle from colliding with a moving obstacle vehicle. From these studies, although the MPC controller shows good performance, some shortcomings remain for the path tracking control of intelligent vehicle. Because the model predictive controller is directly controlled from the perspective of the vehicle state, although the MPC controller has certain predictive ability, the predictive ability of the controller is not the preview operation from the particularity of the preview driving characteristics of the vehicle.

To fully retain the advantages of the MPC controller and simultaneously exert the preview characteristic of the intelligent vehicle to improve the path tracking effect, this work proposes a model predictive control with adaptive preview characteristics and an algorithm of longitudinal vehicle speed-assisted constraint for the path tracking algorithm. The algorithm mainly consists of two parts. The main part is the MPC controller with adaptive preview characteristic. The longitudinal vehicle speed-assisted constraint algorithm is a supplementary part of the algorithm to constrain the MPC controller. First, an MPC control algorithm based on an adaptive preview characteristic of the lateral error and target curvature is proposed to improve the tracking performance. Then, this work builds the basic framework of MPC. The lateral acceleration should be constrained in the MPC controller, the vehicle may understeer, and the tracking performance may deteriorate under constraint. Hence, a longitudinal vehicle speed control assistant algorithm based on the largest ideal lateral acceleration is proposed to address the contradiction and improve the vehicle safety and passability.

This work is organized as follows. Section II describes the autonomous vehicle path tracking model and predictive plant (vehicle dynamic model) for MPC path tracking. Section III builds the model predictive control with adaptive preview characteristics and the longitudinal vehicle speed-assisted constraint for the path tracking algorithm. The several simulations in the Simulink/CARSIM are conducted in Section IV, and Section V provides the conclusions.

II. MODELING

In this part, the autonomous vehicle path tracking model and coordinate systems are described to unify expressions in the full text. Next, an improved vehicle dynamic model based on a three-degree-of-freedom (DOF) vehicle dynamic model was presented to provide a predictive plant for MPC control.

A. AUTONOMOUS VEHICLE PATH TRACKING MODEL

For an autonomous vehicle path tracking model, there are two coordinate systems: Ground coordinate system (GCS) and Vehicle coordinate system, which are fixed with the ground and autonomous vehicle, respectively. Figure 1 also shows many fundamental variables such as the horizontal and vertical coordinates, heading angles and errors. In the field of autonomous vehicle path tracking, the mostly closed-loop control algorithms are based on errors, including the position error, lateral position error and heading angle error [24], [25]. Those errors are commonly calculated from the variables of GCS. Then, lateral position error e_1 and heading angle error e_2 are defined as

$$dY = Y_o - Y_r \tag{1}$$
$$dX = X_o - X_r \tag{2}$$
$$e_1 = dY \times \cos\psi_{des} - dX \times \sin\psi_{des} \tag{3}$$
$$e_2 = \psi - \psi_{des} \tag{4}$$
$$\dot{e}_1 = V_{Ox} \times \sin e_2 \tag{5}$$
$$\dot{e}_2 = \dot{\psi} - \dot{\psi}_{des} \tag{6}$$

where X_r and Y_r are the reference horizontal and vertical coordinates of the center of the vehicle, respectively; ψ_{des} is the reference heading angle; X_o and Y_o are the real horizontal and vertical coordinates of the center of the vehicle, respectively; $\dot{e}_1$ and $\dot{e}_2$ are the change ratio of the lateral position error and heading angle error, respectively; V_{ox} is the longitudinal velocity; $\dot{\psi}$ is the yaw angular velocity of the vehicle; $\dot{\psi}_{des}$ is the reference yaw angular velocity of the vehicle, and $\dot{\psi}_{des} = V_{OX\ des} \times \rho_r$; ρ_r is the desired road curvature.

B. PREDICTIVE PLANT (VEHICLE DYNMIC MODEL) FOR MPC PATH TRACKING

A vehicle is a highly complicated system with multiple degrees of freedom, so it is difficult to model [26]. To simplify the model, there are several assumptions as follows.

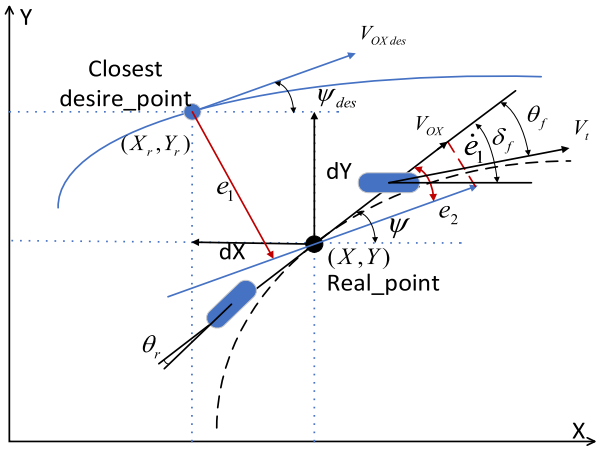

FIGURE 1. Autonomous vehicle path tracking model.

1. The movement of the vehicle in the Z-axis direction is ignored; only the movement in the XY horizontal plane is considered.
2. The bicycle model is used to describe the vehicle movement with negligible load transfer between left and right.
3. The speed of the vehicle slowly changes; the transfer of front and rear axle loads is ignored.
4. The body and suspension systems are rigid.
5. Considering the characteristics of only purely biased tires only, the longitudinal and lateral coupling of tire forces are ignored.
6. The performances of aerodynamics are ignored.

Next, as shown in Figure 1, the vehicle model only has three degrees of freedom: lateral motion, yaw motion about the z-axis and longitudinal motion along the x-axis. According to Newton's second law, the force analysis along the x-axis, y-axis and z-axis includes

$$ma_x = F_{xf} + F_{xr} \tag{7}$$
$$ma_y = F_{yf} + F_{yr} \tag{8}$$
$$I_z\ddot{\psi} = l_f F_{yf} - l_r F_{yr} \tag{9}$$

where a_x and a_y are the longitudinal and lateral acceleration of the vehicle, respectively; F_{xf} and F_{xr} are the longitudinal tire force of the front and rear axles, respectively; F_{yf} and F_{yr} are the lateral tire forces of the front and rear axles, respectively; m and I_z are the vehicle mass and yaw inertia; l_f and l_r are the distances from the center of gravity to the front and rear axles, respectively.

The acceleration in the y-axis direction is

$$a_y = \ddot{y} + V_{ox}\dot{\psi} \tag{10}$$

where $\dot{\psi}$ is the yaw angular velocity.

When subjected to lateral pressure, the tire will produce a small lateral slip angle while generating a corresponding lateral force. The lateral forces in the front and rear axles are

$$F_{yf} = 2C_f(\delta_f - \theta_f) \tag{11}$$
$$F_{yr} = 2C_r(-\theta_r) \tag{12}$$

where C_f and C_r are the lateral stiffnesses of the front and rear axles, and δ_f is the steering angle of the front wheel.

From the geometric perspective, there are the following relationships

$$\tan(\theta_f) = \frac{V_{oy} + l_f\dot{\psi}}{V_{ox}} \tag{13}$$
$$\tan(\theta_r) = \frac{V_{oy} - l_r\dot{\psi}}{V_{ox}} \tag{14}$$

Because angles θ_f and θ_r are small and $V_{oy} = \dot{y}$, we have

$$\theta_f = \frac{\dot{y} + l_f\dot{\psi}}{V_{ox}} \tag{15}$$
$$\theta_r = \frac{\dot{y} - l_r\dot{\psi}}{V_{ox}} \tag{16}$$

Then, the dynamic model can be obtained by merging those formulas as follows

$$\frac{d}{dt}\begin{bmatrix}\dot{y}\\ \dot{\psi}\end{bmatrix} = \boldsymbol{Af}\begin{bmatrix}\dot{y}\\ \dot{\psi}\end{bmatrix} + \boldsymbol{Bf}[\delta_f]$$
$$\begin{bmatrix}\dot{y}\\ \dot{\psi}\end{bmatrix} = \begin{bmatrix}1 & 0\\ 0 & 1\end{bmatrix}\begin{bmatrix}\dot{y}\\ \dot{\psi}\end{bmatrix} \tag{17}$$

where

$$\boldsymbol{Af} = \begin{bmatrix}-\frac{2C_f+2C_r}{mV_{ox}} & -V_{ox} - \frac{2C_f l_f - 2C_r l_r}{mV_{ox}}\\ -\frac{2C_f l_f - 2C_r l_r}{I_z V_{ox}} & -\frac{2C_f l_f^2 + 2C_r l_r^2}{I_z V_{ox}}\end{bmatrix}$$
$$\boldsymbol{Bf} = \begin{bmatrix}\frac{2C_f}{m}\\ \frac{2C_f l_f}{I_z}\end{bmatrix}.$$

By introducing output variable $\dot{\psi}_{des}$, the above model is transformed from a two-output space state equation into a three-output space state equation as

$$\frac{d}{dt}\begin{bmatrix}\dot{y}\\ \dot{\psi}\end{bmatrix} = \boldsymbol{As}\begin{bmatrix}\dot{y}\\ \dot{\psi}\end{bmatrix} + \boldsymbol{Bs}\begin{bmatrix}\delta_f\\ \dot{\psi}_{des}\end{bmatrix}$$
$$\begin{bmatrix}\dot{y}\\ \dot{\psi}\\ \dot{\psi}_{des}\end{bmatrix} = \begin{bmatrix}1 & 0\\ 0 & 1\\ 0 & 0\end{bmatrix}\begin{bmatrix}\dot{y}\\ \dot{\psi}\end{bmatrix} + \begin{bmatrix}0 & 0\\ 0 & 0\\ 0 & 1\end{bmatrix}\begin{bmatrix}\delta_f\\ \dot{\psi}_{des}\end{bmatrix}$$
$$= \boldsymbol{Cs}\begin{bmatrix}\dot{y}\\ \dot{\psi}\end{bmatrix} + \boldsymbol{Ds}\begin{bmatrix}\delta_f\\ \dot{\psi}_{des}\end{bmatrix} \tag{18}$$

where

$$\boldsymbol{As} = \boldsymbol{Af}$$
$$\boldsymbol{Bs} = \begin{bmatrix}\frac{2C_f}{m} & 0\\ \frac{2C_f l_f}{I_z} & 0\end{bmatrix}.$$

According to the autonomous vehicle path tracking model, when heading angle error e_2 is small, the following equation holds

$$\begin{bmatrix}\dot{e}_1\\ \dot{e}_2\end{bmatrix} = \begin{bmatrix}0 & V_{ox}\\ 0 & 0\end{bmatrix}\begin{bmatrix}e_1\\ e_2\end{bmatrix} + \begin{bmatrix}1 & 0 & 0\\ 0 & 1 & -1\end{bmatrix}\begin{bmatrix}\dot{y}\\ \dot{\psi}\\ \dot{\psi}_{des}\end{bmatrix}$$
$$= \boldsymbol{Aa}\begin{bmatrix}e_1\\ e_2\end{bmatrix} + \boldsymbol{Ba}\begin{bmatrix}\dot{y}\\ \dot{\psi}\\ \dot{\psi}_{des}\end{bmatrix} \tag{19}$$

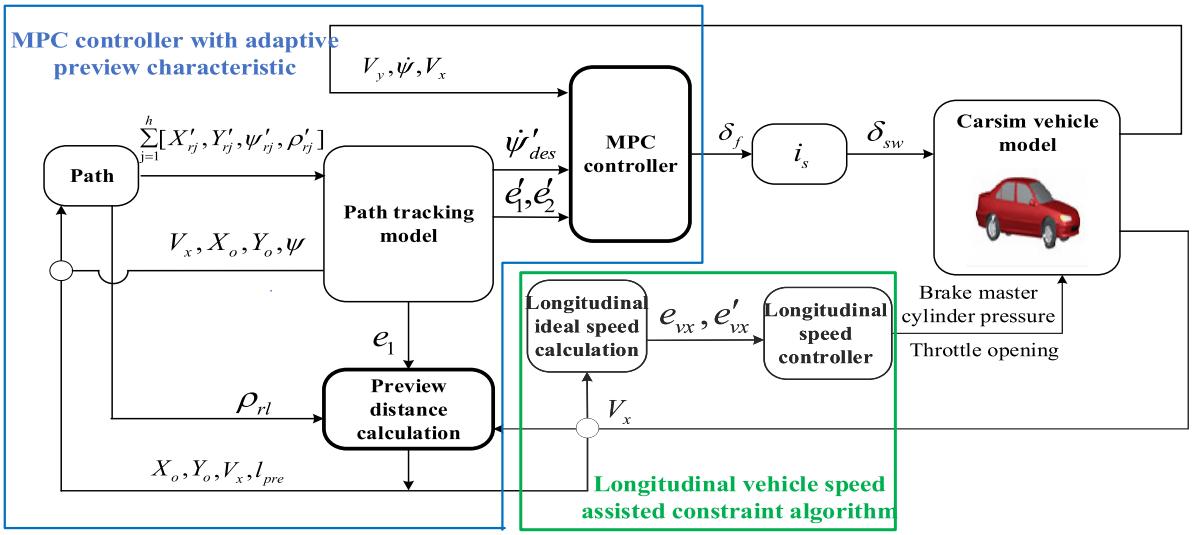

FIGURE 2. Entire framework of the path tracking control algorithm.

Combining state quantities $[\dot{y},\ \dot{\psi}\ ]^T$ and $[\,e_1,\ e_2\,]^T$, the final state space equation is

$$\frac{d}{dt}\begin{bmatrix}\dot{y}\\ \dot{\psi}\\ e_1\\ e_2\end{bmatrix} = \begin{bmatrix}\boldsymbol{As} & \boldsymbol{zeros(2,\,2)}\\ \boldsymbol{Ba}*\boldsymbol{Cs} & \boldsymbol{Aa}\end{bmatrix}\begin{bmatrix}\dot{y}\\ \dot{\psi}\\ e_1\\ e_2\end{bmatrix} + \begin{bmatrix}\boldsymbol{Bs}\\ \boldsymbol{Ba}*\boldsymbol{Ds}\end{bmatrix}\begin{bmatrix}\delta_f\\ \dot{\psi}_{des}\end{bmatrix} = \boldsymbol{A}\begin{bmatrix}\dot{y}\\ \dot{\psi}\\ e_1\\ e_2\end{bmatrix} + \boldsymbol{B1}\left[\delta_f\right] + \boldsymbol{B2} \tag{20}$$

$$\begin{bmatrix}e_1\\ e_2\end{bmatrix} = \begin{bmatrix}0 & 0 & 1 & 0\\ 0 & 0 & 0 & 1\end{bmatrix}\begin{bmatrix}\dot{y}\\ \dot{\psi}\\ e_1\\ e_2\end{bmatrix} = \boldsymbol{C}\begin{bmatrix}\dot{y}\\ \dot{\psi}\\ e_1\\ e_2\end{bmatrix}$$

where

$$\boldsymbol{A} = \begin{bmatrix}-\frac{2C_f+2C_r}{mV_{ox}} & -V_{ox}-\frac{2C_fl_f-2C_rl_r}{mV_{ox}} & 0 & 0\\ -\frac{2C_fl_f-2C_rl_r}{I_zV_{ox}} & -\frac{2C_fl_f^2+2C_rl_f^2}{I_zV_{ox}} & 0 & 0\\ 1 & 0 & 0 & V_{ox}\\ 0 & 1 & 0 & 0\end{bmatrix}$$

$$\boldsymbol{B1} = \begin{bmatrix}\frac{2C_f}{m}\\ \frac{2C_fl_f}{I_z}\\ 0\\ 0\end{bmatrix},\ \boldsymbol{B2} = \begin{bmatrix}0\\ 0\\ 0\\ -\dot{\psi}_{des}\end{bmatrix}$$

After being built, the model should be discretized. This study uses the bilinear transformation to solve:

$$\boldsymbol{A}_{k,t} = (\boldsymbol{I} - \frac{T}{2}\boldsymbol{A})^{-1}(\boldsymbol{I} + \frac{T}{2}\boldsymbol{A}) \tag{21}$$

$$\boldsymbol{B1}_{k,t} = T\boldsymbol{B1} \tag{22}$$

$$\boldsymbol{B2}_{k,t} = T\boldsymbol{B2} \tag{23}$$

$$\boldsymbol{C}_{k,t} = \boldsymbol{C} \tag{24}$$

where T is the model discretized step; $\boldsymbol{I}$ is a 4∗4 unit matrix.

Finally, the discretized state space equation for application is

$$\begin{aligned}\dot{\boldsymbol{x}}_{k,t} &= \boldsymbol{A}_{k,t}\boldsymbol{x}_{k,t} + \boldsymbol{B1}_{k,t}u_{k,t} + \boldsymbol{B2}_{k,t}\\ \boldsymbol{y}_{k,t} &= \boldsymbol{C}_{k,t}\boldsymbol{x}_{k,t}\end{aligned} \tag{25}$$

III. PARTH TRACKING CONTROL ALGRITHM

To introduce the driver preview characteristics into the path tracking control using the MPC controller, we analyzed the characteristics of the traditional MPC and established an adaptive preview strategy based on the MPC controller. Next, the MPC basic framework was established. Finally, to avoid the problem that understeer is easily caused by the constrained lateral acceleration in MPC, we proposed a longitudinal vehicle speed-assisted constraint strategy based on the lateral acceleration constraint. The entire framework of the path tracking control algorithm is shown in Figure 2.

A. ADAPTIVE PREVIEW STRATEGY BASED ON THE MPC CONTROLLER

During the actual driving process, the drivers do not start steering after entering the curve. Instead, the drivers start steering before entering the curve. This process is called the driver preview operation. For path tracking based on traditional MPC controllers, there is no preview operation in the tracking process. To make the driving process more realistic, driving characteristics with a preview operation are added to improve the tracking performance, an adaptive preview strategy based on the MPC controller was proposed.

REMARK 1: MPC CONTROLLER WITH PREVIEW DRIVING CHARACTERISTIC

For a tracking control issue, reference states can be divided into two types: control reference state and result reference state. From the perspective of the control principle, the traditional MPC controller adopts the current states and reference variables that correspond to the current states as the basis of the control, where the control reference state point is identical to the result reference state point. As shown in Figure 3, when the vehicle is at position (X_O^k, Y_O^k), its control and result reference states correspond to the states of the vehicle at the closest point (X_r^k, Y_r^k) to the vehicle. Figure 4 is a corresponding diagram of the MPC control reference states.

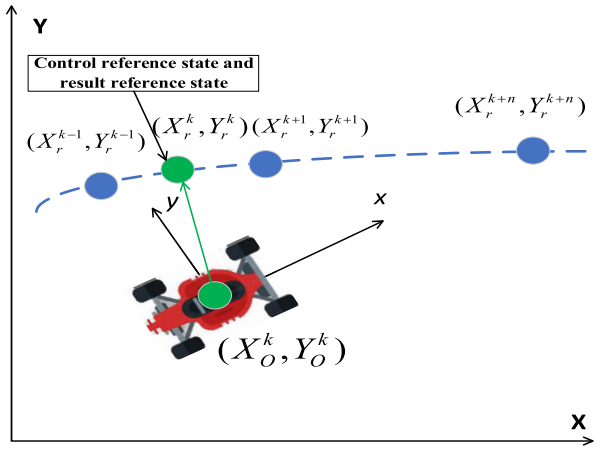

FIGURE 3. Status quantity correspondence diagram.

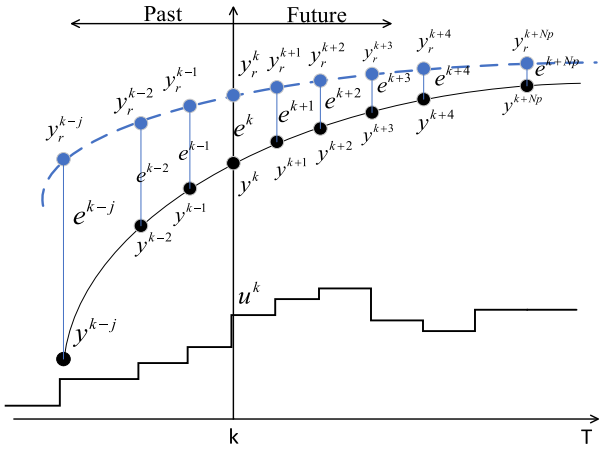

FIGURE 4. Traditional MPC control reference correspondence diagram.

Based on the analysis of the reference state selected by the traditional MPC controller, an MPC controller with a preview strategy was proposed for the problem that there was no preview operation using the traditional MPC controller. In the MPC controller with a preview strategy, the closest point (X_r^k, Y_r^k) to the vehicle is not the control reference state point but only a result reference point. Reference point (X_r^{k+i}, Y_r^{k+i}) at a certain distance in front of the vehicle is selected as the control reference state point of (X_O^k, Y_O^k). The MPC control process transits to that in Figure 5, where i is the preview time. The modified MPC control process only changes the current control reference state. We can consider that the actual states under the original MPC reference states at K time generate an offset, which will not affect the control stability and control mode of the MPC [27].

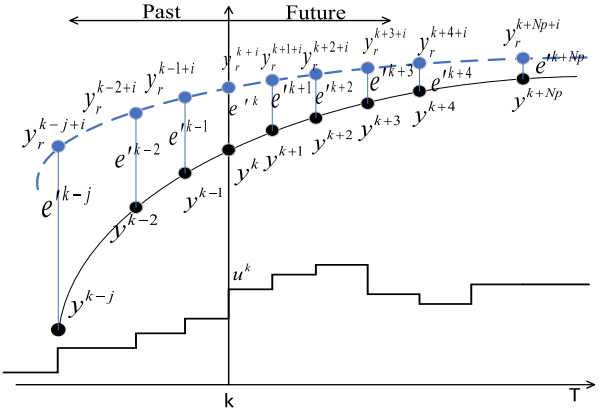

FIGURE 5. Reference map of the MPC controller with preview driving characteristic.

REMARK 2: ADAPTIVE PREVIEW STRATATEGY

In real life, the drivers generally adjust their driving behavior through the current state of the vehicle and the road ahead, including the driving distance, steering behavior and driving speed. During the driving process of the driver, the driving accuracy is controlled in a safety zone for a specified path tracking. In addition, steering ahead is adopted to enable the vehicle to quickly enter the desired states, and the steering rate of change is minimized to improve driving comfort. The action of steering ahead is started depending on the preview distance, which becomes the key to affect the lateral control performance. During the driving process, the preview distance should be changeable because the preview distance will decrease if the driver encounters an increase in curvature of the front path. Simultaneously, to ensure the control accuracy, the preview distance will also decrease when the error increases. Therefore, an adaptive preview distance strategy based on the target curvature and lateral error was proposed

$$t_{pre\max} = 0.02V_{OX} \tag{26}$$

$$t_{pre\min} = 0.016V_{OX} \tag{27}$$

$$\begin{cases} t_{pre} = t_{pre\max} - K_1 t_{pre\max} \bullet (\frac{|e_1|}{|e_{\max}|}) - \\ \quad K_2 t_{pre\max} \bullet (\frac{|\rho|}{|\rho_{\max}|}), \quad if \quad t_{pre} > t_{pre\min} \\ t_{pre} = t_{pre\min} \quad , \quad if \quad t_{pre} \le t_{pre\min} \end{cases} \tag{28}$$

$$L_{pre} = V_{OX} t_{pre} \tag{29}$$

where $K_1 + K_2 = 1$ and K_1 and K_2 are the weight coefficients; e_{max} is the maximal lateral error; ρ_{max} is the maximal path curvature; t_{premax} and t_{premin} are the maximal and minimal preview time; L_{pre} is the preview distance.

REMARK 3: MPC CONTROLLER MPC WITH ADAPTIVE PREVIEW STRATATEGY

The reference point at the front of the vehicle, which is obtained by the adaptive preview distance L_{pre}, was used as the control reference point of the MPC controller, and the closest point was used as the result reference point. In summary, the MPC controller with adaptive preview strategy can be represented by Figures 6 and 7.

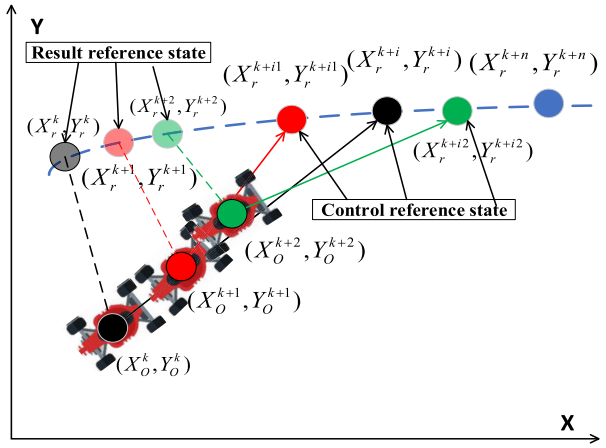

FIGURE 6. Schematic diagram of the MPC controller with adaptive preview strategy.

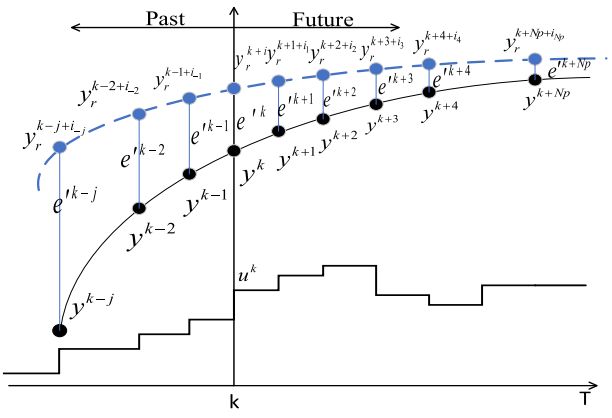

FIGURE 7. Corresponding diagram of the MPC controller with adaptive preview strategy.

B. BASIC MPC FRAMEWORK FOR PATH TRACKING

REMARK 1: BUILDING THE PREDICTION EQUATION

We converted equation (25) to an augmented matrix form, whose state quantities are $\boldsymbol{\xi}(k) = [\boldsymbol{x}(k),\ u(k)]^T$ and control quantity is $\Delta u(k)$.

$$\begin{aligned}\boldsymbol{\xi}(k+1|k) &= \tilde{\boldsymbol{A}}_{k,t}\boldsymbol{\xi}(k|k) + \tilde{\boldsymbol{B}}1_{k,t}\Delta u(k|k) + \tilde{\boldsymbol{B}}2_{k,t}\\ \boldsymbol{\eta}(k+1|k) &= \tilde{\boldsymbol{C}}_{k,t}\boldsymbol{\xi}(k|k)\end{aligned} \tag{30}$$

where $\tilde{\boldsymbol{A}}_{k,t} = \begin{bmatrix}\boldsymbol{A}_{k,t} & \boldsymbol{B}1_{k,t}\\ \boldsymbol{0}_{m\times n} & \boldsymbol{I}_m\end{bmatrix}, \tilde{\boldsymbol{B}}1_{k,t} = \begin{bmatrix}\boldsymbol{B}1_{k,t}\\ \boldsymbol{I}_m\end{bmatrix}, \tilde{\boldsymbol{B}}2_{k,t} = \begin{bmatrix}\boldsymbol{B}2_{k,t}\\ \boldsymbol{0}_m\end{bmatrix}, \tilde{\boldsymbol{C}}_{k,t} = [\boldsymbol{C}_{k,t}\ 0]$.

To further simplify the expression, we make those definitions as follows

$$\tilde{\boldsymbol{A}} = \tilde{\boldsymbol{A}}_{k,t}, k = 1, 2, \cdots, t+N-1 \tag{31}$$

$$\tilde{\boldsymbol{B}}1 = \tilde{\boldsymbol{B}}1_{k,t}, k = 1, 2, \cdots, t+N-1 \tag{32}$$

$$\tilde{\boldsymbol{B}}2 = \tilde{\boldsymbol{B}}2_{k,t}, k = 1, 2, \cdots, t+N-1 \tag{33}$$

$$\tilde{\boldsymbol{C}} = \tilde{\boldsymbol{C}}_{k,t}, k = 1, 2, \cdots, t+N-1 \tag{34}$$

Then, the predictive horizon and control horizon are set as N_P and N_C. Therefore, the state quantity and system output in the prediction horizon are

$$\begin{aligned}\boldsymbol{\xi}(k+N_p|k) &= \tilde{\boldsymbol{A}}^{Np}\boldsymbol{\xi}(k|k) + \tilde{\boldsymbol{A}}^{Np-1}\tilde{\boldsymbol{B}}1\Delta u(k|k) + \cdots\\ &\quad + \tilde{\boldsymbol{A}}^{Np-Nc-1}\tilde{\boldsymbol{B}}1\Delta u(k+N_c|k) + \tilde{\boldsymbol{A}}^{Np-1}\tilde{\boldsymbol{B}}2_1\\ &\quad + \cdots\tilde{\boldsymbol{A}}\tilde{\boldsymbol{B}}2_{Np-1} + \tilde{\boldsymbol{B}}2_{Np}\\ \boldsymbol{\eta}(k+N_p|k) &= \tilde{\boldsymbol{C}}\tilde{\boldsymbol{A}}^{Np}\xi(k|k) + \tilde{\boldsymbol{C}}\tilde{\boldsymbol{A}}^{Np-1}\tilde{\boldsymbol{B}}1\Delta u(k|k)\\ &\quad + \cdots + \tilde{\boldsymbol{C}}\tilde{\boldsymbol{A}}^{Np-Nc-1}\tilde{\boldsymbol{B}}1\Delta u(k+N_c|k)\end{aligned} \tag{35}$$

Next, the form of the output matrix of the system at the future time is expressed as

$$\boldsymbol{Y}(k) = \boldsymbol{\Psi}_k\boldsymbol{\xi}(k|k) + \boldsymbol{\Theta}_k\boldsymbol{\Delta U}(k|k) + \boldsymbol{\Gamma}_k \tag{36}$$

where $\boldsymbol{Y}(k) = \begin{bmatrix}\boldsymbol{\eta}(k+1|k)\\ \boldsymbol{\eta}(k+2|k)\\ \vdots\\ \boldsymbol{\eta}(k+N_p|k)\end{bmatrix}, \boldsymbol{\Psi}_k = \begin{bmatrix}\tilde{\boldsymbol{C}}\tilde{\boldsymbol{A}}\\ \tilde{\boldsymbol{C}}\tilde{\boldsymbol{A}}^2\\ \vdots\\ \tilde{\boldsymbol{C}}\tilde{\boldsymbol{A}}^{Np}\end{bmatrix}, \boldsymbol{\Delta U}(k) = \begin{bmatrix}\Delta u(k|k)\\ \Delta u(k+1|k)\\ \vdots\\ \Delta u(k+N_c|k)\end{bmatrix}, \boldsymbol{\Gamma}_k = \begin{bmatrix}\tilde{\boldsymbol{B}}2\\ \tilde{\boldsymbol{A}}\tilde{\boldsymbol{B}}2 + \tilde{\boldsymbol{B}}2\\ \vdots\\ \tilde{\boldsymbol{A}}^{N_p-1}\tilde{\boldsymbol{B}}2 + \cdots + \tilde{\boldsymbol{A}}\tilde{\boldsymbol{B}}2 + \tilde{\boldsymbol{B}}2\end{bmatrix}$,

$$\boldsymbol{\Theta}_k = \begin{bmatrix}\tilde{\boldsymbol{C}}\tilde{\boldsymbol{B}}1 & 0 & \cdots & 0\\ \tilde{\boldsymbol{C}}\tilde{\boldsymbol{A}}\tilde{\boldsymbol{B}}1 & \tilde{\boldsymbol{C}}\tilde{\boldsymbol{B}}1 & \cdots & 0\\ \vdots & \vdots & \ddots & \vdots\\ \tilde{\boldsymbol{C}}\tilde{\boldsymbol{A}}^{N_c-1}\tilde{\boldsymbol{B}}1 & \tilde{\boldsymbol{C}}\tilde{\boldsymbol{A}}^{N_c-2}\tilde{\boldsymbol{B}}1 & \cdots & \tilde{\boldsymbol{C}}\tilde{\boldsymbol{B}}1\\ \tilde{\boldsymbol{C}}\tilde{\boldsymbol{A}}^{N_c}\tilde{\boldsymbol{B}}1 & \tilde{\boldsymbol{C}}\tilde{\boldsymbol{A}}^{N_c-1}\tilde{\boldsymbol{B}}1 & \cdots & \tilde{\boldsymbol{C}}\tilde{\boldsymbol{A}}\tilde{\boldsymbol{B}}1\\ \vdots & \vdots & \ddots & \vdots\\ \tilde{\boldsymbol{C}}\tilde{\boldsymbol{A}}^{N_p-1}\tilde{\boldsymbol{B}}1 & \tilde{\boldsymbol{C}}\tilde{\boldsymbol{A}}^{N_p-2}\tilde{\boldsymbol{B}}1 & \cdots & \tilde{\boldsymbol{C}}\tilde{\boldsymbol{A}}^{N_p-N_c-1}\tilde{\boldsymbol{B}}1\end{bmatrix}$$

REMARK 2: BUILDING THE COST FUNTION

When constructing the cost function, we considered that if the control quantity was used as the state quantity, the control increment could not be precisely constrained. Simultaneously, considering the feasible solution to ensure the optimization goal, we added a relaxation factor and constructed the tracking cost function as

$$\begin{aligned}&J(\boldsymbol{\xi}(k), u(k-1), \boldsymbol{\Delta U}(k))\\ &\quad = \sum_{i=1}^{N_p}||\boldsymbol{\eta}(k+i|k) - \boldsymbol{\eta}_{ref}(k+1|k)||_{\boldsymbol{Q}}^2\\ &\qquad + \sum_{i=1}^{N_c-1}||\Delta u(k+i|k)||_{\boldsymbol{R}}^2 + \tau\varepsilon^2\end{aligned} \tag{37}$$

where ε is the relaxation factor, τ is the weight coefficient, $\boldsymbol{Q}$ is the weight coefficient matrix for state variables, and $\boldsymbol{R}$ is the weight coefficient matrix for control variables.

The deviation of the output in the predicted horizon is obtained by equation (36) as

$$\boldsymbol{E}(k) = \boldsymbol{\Psi}_k \boldsymbol{\xi}(k|k) + \boldsymbol{\Theta}_k \boldsymbol{\Delta U}(k|k) + \boldsymbol{\Gamma}_k - \boldsymbol{Y}_{ref}(k) \quad (38)$$

where $\boldsymbol{Y}_{ref}(k) = [\,\boldsymbol{\eta}_{ref}(k+1|k), \cdots, \boldsymbol{\eta}_{ref}(k+N_p|k)\,]^T$, $\boldsymbol{\eta}_{ref}(k+i|k)$ is the reference output at step $k+i$.

To simplify the expression, the equation of $\boldsymbol{\Psi}_k \boldsymbol{\xi}(k|k) + \boldsymbol{\Gamma}_k - \boldsymbol{Y}_{ref}(k)$ is defined as $\boldsymbol{E}_{eq}(k)$. Therefore, the cost function can be further expressed as

$$\begin{aligned} &J(\boldsymbol{\xi}(k), u(k-1), \boldsymbol{\Delta U}(k)) \\ &\quad = [\boldsymbol{\Delta U}(k); \varepsilon]^T \boldsymbol{H}_k [\boldsymbol{\Delta U}(k); \varepsilon] \\ &\qquad + \boldsymbol{F}_k [\boldsymbol{\Delta U}(k); \varepsilon] + \boldsymbol{E}_{eq}^T(k) \boldsymbol{Q} \boldsymbol{E}_{eq}(k) \end{aligned} \quad (39)$$

where $\boldsymbol{H}_k = \begin{bmatrix} \boldsymbol{\Theta}_k^T \boldsymbol{Q} \boldsymbol{\Theta}_k + \boldsymbol{R} & 0 \\ 0 & \tau \end{bmatrix}$, $\boldsymbol{F}_k = \begin{bmatrix} 2\boldsymbol{E}_{eq}^T(k) \boldsymbol{Q} \boldsymbol{\Theta}_k & 0 \end{bmatrix}$.

REMARK 3: SETTING THE STABILITY CONSTRAINTS

The dynamic vehicle model considering the internal forces, energy or momentum in the system [3], [28], [29] is built based on the assumptions in Section II. Thus, the constraints should include the steering angle, change ratio of the steering angle, tire lateral slip angle, and ground attachment conditions.

The steering wheel of the vehicle was turned to the left and right limit positions, i.e., ±540°. The steering ratio of the vehicle was set as 16.5, so the limit position of the front wheel was ±32.75°. According to the limit experiment of the current steering wheel of the motor, the limit steering speed of the general vehicle was 500°/*s*; to ensure the steer speed, the value range was generally [250°/*s*, 500°/*s*]. After converting the units according to the actual control step, the constraint of the steering wheel angle was set as [-0.5] $\leq U_k \leq$ [0.5], and the change ratio of the steering wheel angle was set as $[-0.005] \leq \Delta U_k^* \leq [0.005]$.

In addition, according to the tire's characteristics, when the lateral slip angle of the tire is within [-5°, 5°], the lateral slip angle is linear with the slip bias force, and the vehicle is in a stable state in the lateral direction. The dynamic model was based on the assumption of a small lateral slip angle, so the constraint on the front wheel slip angle was defined as -5° $\leq a_f \leq$ 5°. In tire dynamics, there is the following relationship

$$\alpha_f = \frac{\dot{y} + l_f \dot{\psi}}{V_{Ox}} - \delta_f \quad (40)$$

Therefore, $-5° \leq \frac{\dot{y}+l_f\dot{\psi}}{V_{Ox}} - \delta_f \leq 5°$.

During the operation of the vehicle, the vehicle is restricted by ground attachment conditions, and the lateral acceleration is a manifestation of the vehicle attachment conditions. The lateral acceleration can be restricted to achieve the ground attachment conditions. It can increase the safety of the vehicle and improve the comfort of the vehicle when the lateral acceleration is restricted. However, when the lateral acceleration is restrained in the MPC controller, while the vehicle enters the large curvature curve at a constant speed, the steering angle is easily restricted. This scenario may result in an insufficient steering angle, and there is a possibility to rush out of the track path with decrease tracking performance. Aiming at the dilemma between lateral acceleration constraint and large curvature curve under constant speed, a longitudinal speed-assisted constraint algorithm based on lateral acceleration was proposed [30]. The longitudinal speed-assisted constraint is equivalent to the lateral acceleration constraint, which is a supplement constraint of the MPC. The longitudinal speed-assisted constraint algorithm will be explained in detail in part C of this chapter.

REMARK 4: OPTIMIZATION PROBLEM

Combining the above cost function and constraints, the solution process transfers to the following quadratic programming optimization problem

$$\begin{aligned} \min_{\Delta u_k, \varepsilon} \; & = [\boldsymbol{\Delta U}(k); \varepsilon]^T \boldsymbol{H}_k [\boldsymbol{\Delta U}(k); \varepsilon] + \boldsymbol{F}_k [\boldsymbol{\Delta U}(k); \varepsilon] \\ s.t. \quad & \boldsymbol{\Delta U}_{\min} \leq \boldsymbol{\Delta U}_k \leq \boldsymbol{\Delta U}_{\max} \\ & \boldsymbol{U}_{\min} \leq \boldsymbol{U}_k + \boldsymbol{V} \boldsymbol{\Delta U}_k \leq \boldsymbol{U}_{\max} \\ & -\alpha_{f\,\min} + \frac{\boldsymbol{x}(1) + l_f \boldsymbol{x}(2)}{V_{Ox}} \leq \boldsymbol{U}_k + \boldsymbol{V} \boldsymbol{\Delta U}_k \leq -\alpha_{f\,\max} \\ & + \frac{\boldsymbol{x}(1) + l_f \boldsymbol{x}(2)}{V_{Ox}} \boldsymbol{Y}_{\min} - \varepsilon \leq \boldsymbol{Y}_{sc} \leq \boldsymbol{Y}_{\max} + \varepsilon \\ & \varepsilon > 0 \end{aligned} \quad (41)$$

where $\boldsymbol{V} = \underbrace{\begin{bmatrix} 1 & 0 & \cdots & 0 \\ 1 & 1 & \ddots & 0 \\ \vdots & \vdots & \cdots & \vdots \\ 1 & 1 & \cdots & 0 \\ 1 & 1 & \cdots & 1 \end{bmatrix}}_{N_c \times N_c} \otimes \boldsymbol{I}_m$; $\otimes$ is Kronecker product.

REMARK 5: FEEDBACK

After completing the optimization solution in each control cycle, a series of control input increments in the control time domain is obtained

$$\Delta \boldsymbol{U}_k^* = [\Delta u_k^*, \cdots, \Delta u_{k+N_c-1}^*]^T$$

We applied the first element in the control sequence to the system as the actual control input increment; then, the control variable at this step is

$$u(k) = u(k-1) + \Delta u_k^* \quad (42)$$

The system performs the control variable to the next step and repredicts the output of the next step based on the state information at a new step. This cycle is repeated until the entire control process is completed.

C. LONGITUDINAL VEHICLE SPEED-ASSISTED CONSTRAINT ALGORITHM

When the vehicle is running, it is limited by the ground adhesion. The following relationship holds: $\sqrt{a_x^2 + a_y^2} \leq \mu g$. Accordingly, we can derive that $|a_y| \leq \mu g$, where μ is the road surface adhesion coefficient, and the road surface adhesion coefficient is generally in the range of $\mu \in [0.2, 0.85]$. Simultaneously, from the perspective of vehicle

control safety, the range of the lateral acceleration limit is generally $|a_y| \in [4, 6]m/s^2$. Thus, the lateral acceleration limit was taken as 0.6 g, i.e., $-6m/s^2 \leq a_y \leq 6m/s^2$.

In the path tracking control, when the lateral constraint and control precision are contradictory and neither lateral constraint nor control precision is to be relaxed, only the longitudinal speed of the vehicle is decreased to relax the limit condition [31]. For path tracking control research, the goal is to ensure control accuracy under the most extreme conditions possible. In the lateral control constraint, the lateral acceleration is affected by the vehicle speed. According to the kinematic model, when the lateral slope of the road is ignored on the horizontal plane, the lateral acceleration is

$$a_{ydes} = \frac{V_{oxdes}^2}{R_{des}} = V_{oxdes}^2 \rho \tag{43}$$

where a_{ydes} is the ideal lateral acceleration; R_{des} is the ideal turning radius; V_{oxdes} is the ideal speed; ρ is the road curvature.

According to the above formula, the ideal limit speed can be derived. In actual operation, the largest ideal limit speed should be set. Thus, the following expression holds

$$\begin{cases} V_{oxdes} = \sqrt{|\frac{a_{ydes}}{\rho}|}, & if \quad \sqrt{|\frac{a_{ydes}}{\rho}|} \leq V_{oxdes}^{\max} \\ V_{oxdes} = V_{oxdes}^{\max}, & if \quad \sqrt{|\frac{a_{ydes}}{\rho}|} > V_{oxdes}^{\max} \end{cases} \tag{44}$$

To better simulate human driving characteristics, the calculated target speed must be decelerated in advance and accelerated at a delay.

IV. SIMULATION RESULTS AND ILLUSTRATION

A. TRADITIONAL MPC CONTROLLER SIMULATION

REMARK 1: SIMULATION DESCRIPTION

To verify the proposed dynamic model and provide a comparable object using the traditional MPC controller, a cosimulation program was established in Simulink/CARSIM. The program converted the front wheel angle into the steering wheel angle input through the steering system transmission ratio. The longitudinal vehicle speed was set as a constant value in CARSIM. In the program, a C-class car was selected to have the CARSIM's vehicle model, and the other variables are shown in table 1. The running step of the program was set to 1000 Hz, and the control step of the controller was set to 100 Hz.

REMARK 2: SETTING WORKING CONDITION

The ISO3888-1:1999 shifting condition was set as a part of the test path in the middle of a straight road, and its variables are shown in Figure 8.

1—direction of travel, 2—lane offset, 3—road width, 4—road segment 1, 5—road segment 2, 6—road segment 3, 7—road segment 4, 8—road segment 5, 9—road segment 6.

The positions and offsets of each segment in Figure 8 are shown in table 2.

REMARK 3: SIMULATION RESULTS

TABLE 1. Simulation parameters.

Symbol	Interpretation	Value (Unit)
m	Total mass	1300 (kg)
I_Z	Moment of inertia	1523 (kg·m^2)
l_f	Front axle distance	1.01 (m)
l_r	Rear axle distance	1.56 (m)
C_{cf}	Front cornering stiffness	72000 (N/rad)
C_{rf}	Rear cornering stiffness	80000 (N/rad)
T	Model discretized step	0.002 (s)
Np	Predictive horizon	300
Nc	Control horizon	2
$\boldsymbol{Q}$	state weight matrix	[1000 0; 0 1]
$\boldsymbol{R}$	control weight matrix	2000000

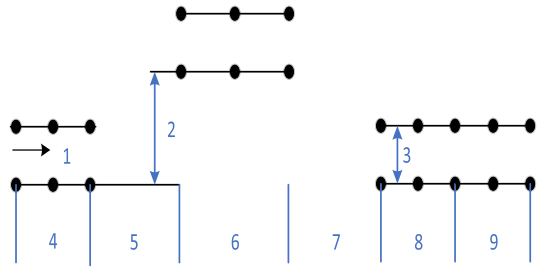

FIGURE 8. ISO3888-1:1999 path settings.

TABLE 2. Table of variables in the ISO3888-1:1999 path settings.

section	Length/m	Offset/m	Width/m
1	15	-	1.1×car width+0.25
2	30	-	——
3	25	3.5	1.2×car width+0.25
4	25	-	——
5	15	-	1.3×car width+0.25
6	15	-	1.3×car width+0.25

The simulation results with longitudinal speeds of 10 m/s, 20 m/s and 30 m/s are shown in Figure 9.

The simulation results show that the largest lateral error of tracking the path is 0.22 m, the largest yaw angle error of tracking the path is -0.040 *rad*, the largest lateral acceleration is -0.198 g, and the largest lateral slip angle of the left front wheel is -0.75° when the vehicle speed is 10 m/s. When the vehicle speed is 20 m/s, the largest lateral error is 0.50 m, the largest yaw angle error of tracking the path is -0.067 *rad*, the largest lateral acceleration is 0.600 g, and the largest lateral slip angle of the left front wheel is -2.37°. When the vehicle speed is 30 m/s, the path tracking performance is obviously worse: the lateral error is 1.46 m, the largest yaw angle error is -0.094 *rad*, the largest lateral acceleration is 0.8461 g, and the largest lateral slip angle of the left front wheel is -4.42°. At low and medium speeds, the tracking performance basically satisfies the tracking requirements, but the tracking performance deteriorates when the vehicle speed increases.

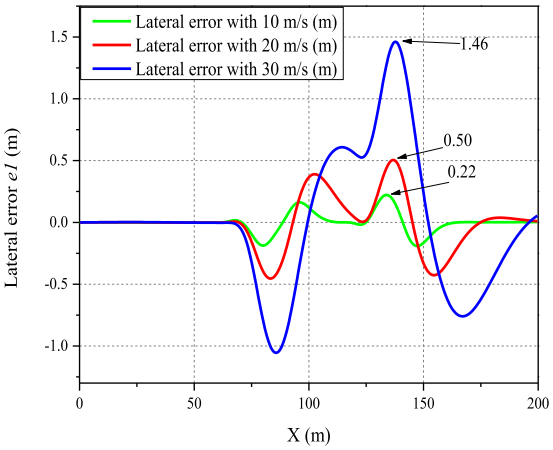

(a). Lateral error at different vehicle speeds

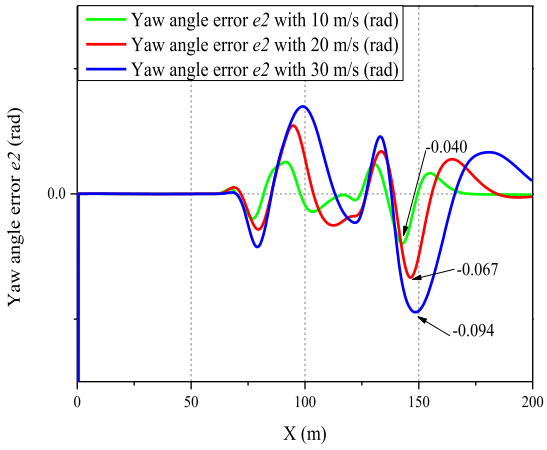

(b). Yaw angle error at different speeds

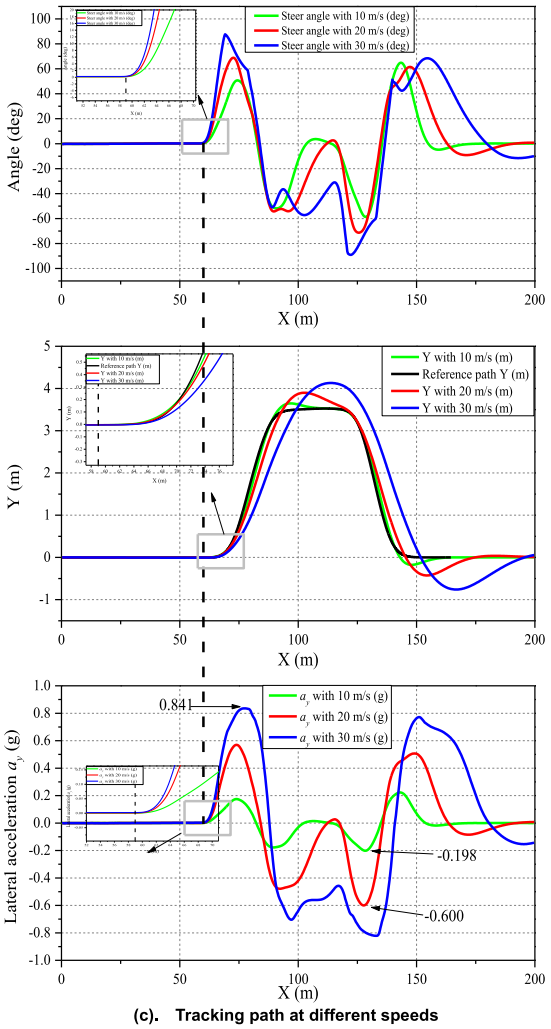

(c). Tracking path at different speeds

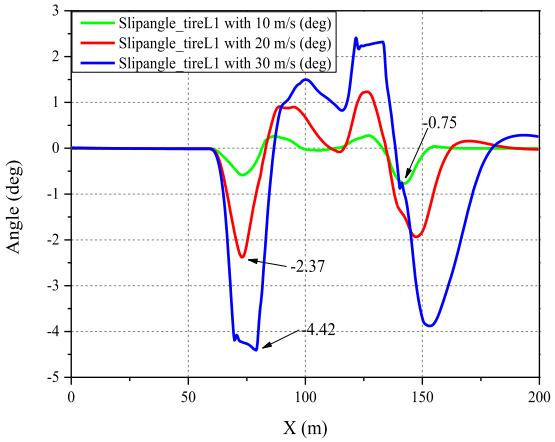

(d). Lateral slip angle of the left front wheel at different speeds

FIGURE 9. (a). Lateral error at different vehicle speeds (b). Yaw angle error at different speeds (c). Tracking path at different speeds (d). Lateral slip angle of the left front wheel at different speeds.

At the first turn in Figure 9 (c), all three steering actions begin only when the vehicle enters the first corner, which is the 59th m in the X axis. In the enlarged part of Figure 9 (c), the tracking actions of the vehicle is gradually delayed when the vehicle speed increases. The tracking action has lagged behind the reference path, which results in a worse tracking performance when the vehicle speed is 30 m/s.

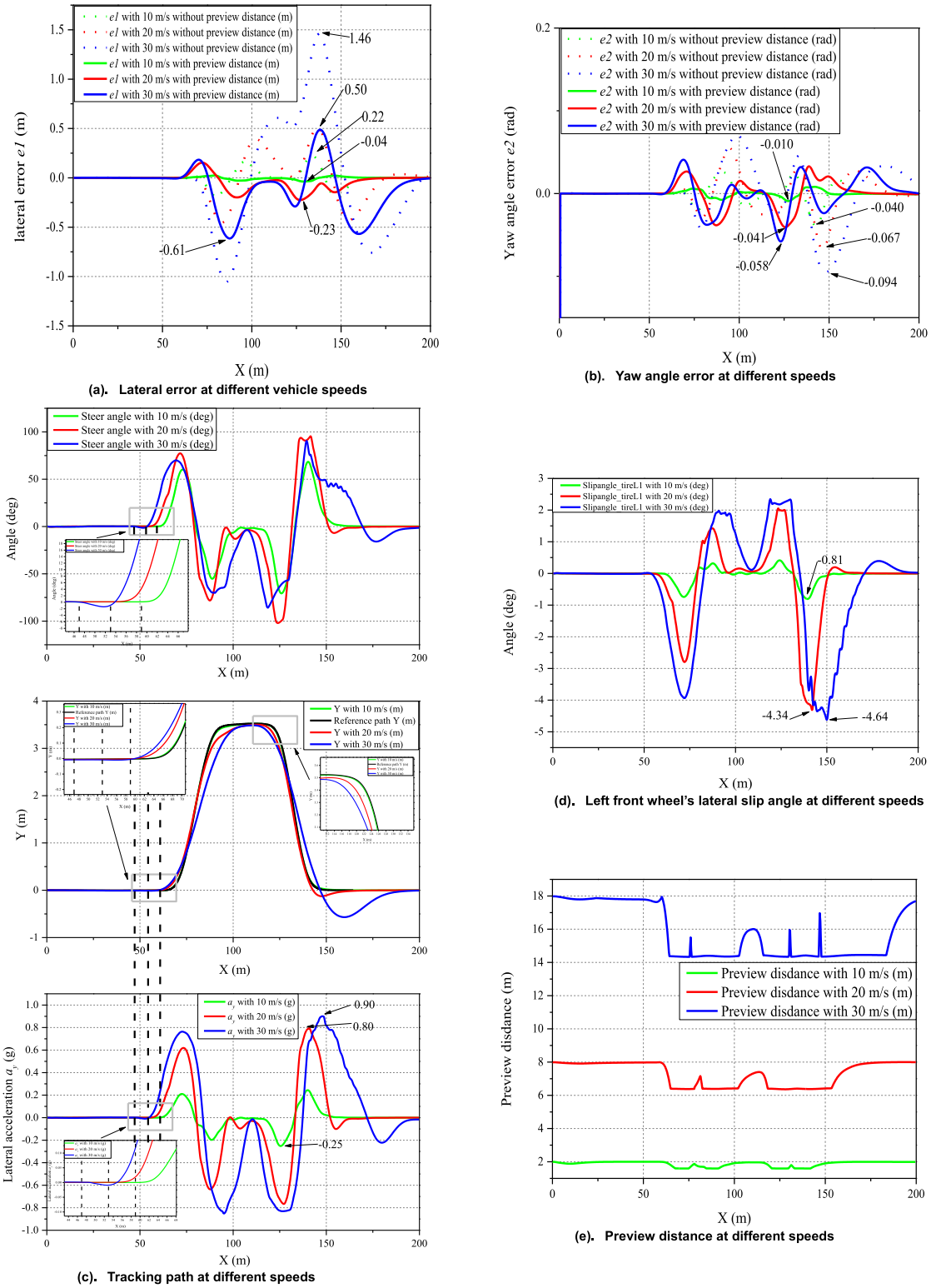

(a). Lateral error at different vehicle speeds

(b). Yaw angle error at different speeds

(c). Tracking path at different speeds

(d). Left front wheel's lateral slip angle at different speeds

(e). Preview distance at different speeds

FIGURE 10. (a). Lateral error at different vehicle speeds (b). Yaw angle error at different speeds (c). Tracking path at different speeds (d). Left front wheel's lateral slip angle at different speeds (e). Preview distance at different speeds.

B. SIMULATION TO VERIFY THE ADAPTIVE PREVIEW STRATATEGY BASED ON THE MPC CONTROLLER

To verify the proposed the adaptive preview strategy based on the MPC controller, we set the double-shifting conditions identical to Section IV.A and the longitudinal speeds to be 10 m/s, 20 m/s, and 30 m/s. The newly added and changed parameters are shown in table 3, and the simulation results are shown in Figure 10.

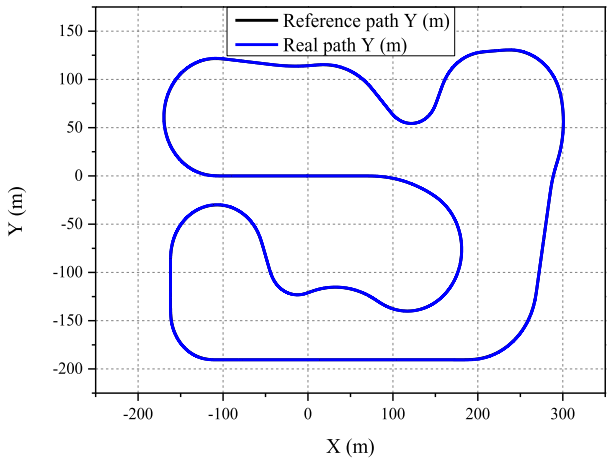

(a). Tracking path

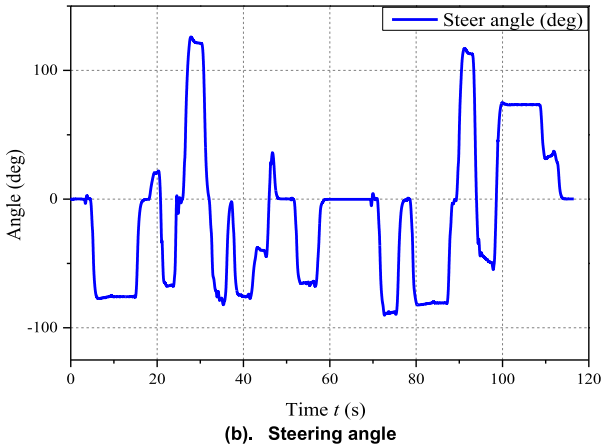

(b). Steering angle

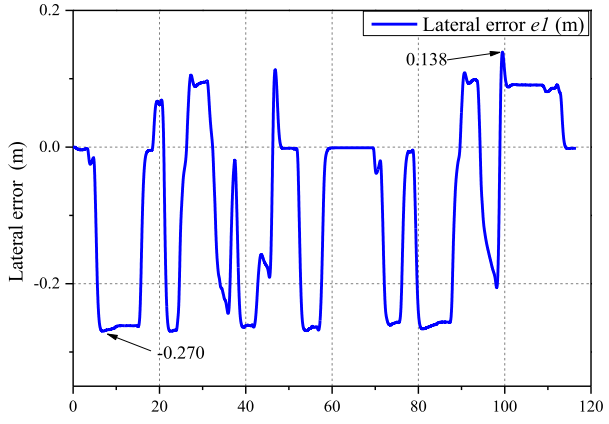

(c). Lateral error

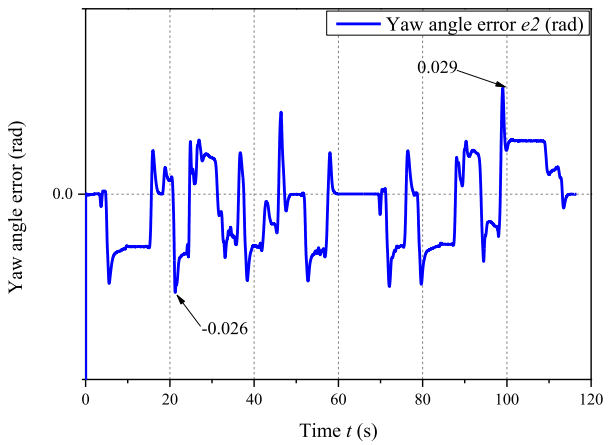

(d). Yaw angle error

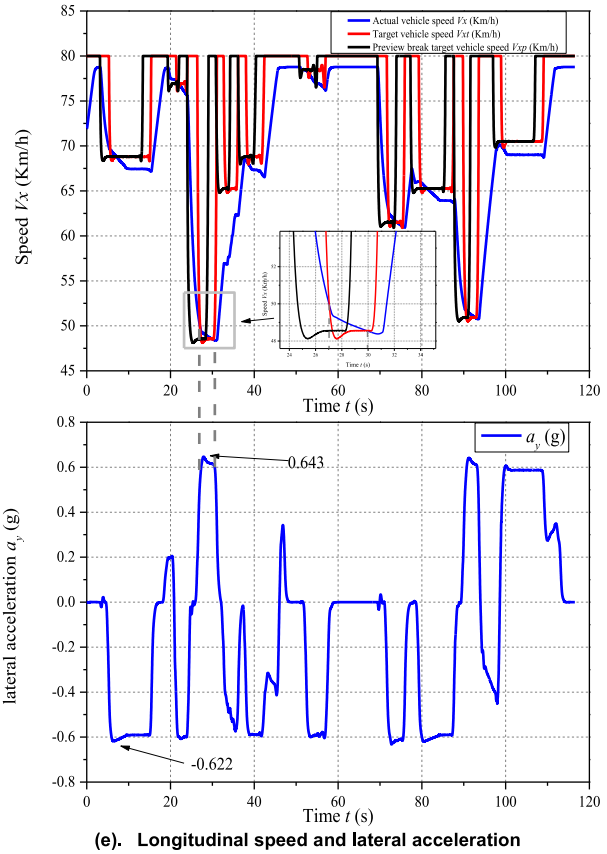

(e). Longitudinal speed and lateral acceleration

FIGURE 11. (a). Tracking path (b). Steering angle (c). Lateral error (d). Yaw angle error (e). Longitudinal speed and lateral acceleration.

As shown in Figure 10, when the vehicle speed is 10 m/s, the largest lateral error of tracking the path is 0.04 m, the largest yaw angle error of tracking the path is -0.010 *rad*, the largest lateral acceleration is -0.25 *g*, and the largest lateral slip angle of the left front wheel is -0.81°. When the vehicle speed is 20 m/s, the largest lateral error is 0.23 m, the largest yaw angle error of tracking the path is -0.041 *rad*, the largest lateral acceleration is 0.80 *g*, and the largest lateral slip angle of the left front wheel is -4.34°. When the vehicle speed is 30 m/s, the largest lateral error is 0.61 m, the largest yaw angle error of tracking the path is -0.058 *rad*, the largest lateral acceleration is 0.90 *g*, and the largest lateral slip angle of the left front wheel is -4.64°. The comparison in Figure 10 (a) shows that the largest lateral error of path tracking is

TABLE 3. Table of new variables in the model.

Symbol	Interpretation	Value (Unit)
K_1	Lateral error weight	0.55
K_2	Path curvature weight	0.45
e_{max}	Largest lateral error	0.2 (m)
ρ_{max}	Largest path curvature	0.04
Np_10	Predictive horizon of 10 m/s	100
Np_20	Predictive horizon of 20 m/s	81
Np_30	Predictive horizon of 30 m/s	70

reduced by 81.8%, 54%, and 58.2% when the vehicle speed is 10 m/s, 20 m/s, and 30 m/s, respectively. The comparison in Figure 10 (b) shows that the largest yaw angle error of path tracking is reduced by 75.0%, 38.8% and 38.3% when the vehicle speed is 10 m/s, 20 m/s, and 30 m/s, respectively.

Figure 10 (e) shows that the preview distance varies with the curvature and lateral error at different vehicle speeds. Therefore, as shown in the enlarged area in Figure 10 (c), the steering action starts before entering the curve and advances when the vehicle speed increases. We specifically present three steering actions that begins at the 59^{th} m, 53^{th} m and 47^{th} m on the X axis. The simulation results show that the tracking performance was improved, but the lateral acceleration of the vehicle was easily at the extreme edge.

C. SIMULATION TO VERIFY THE PROPOSED PATH TRACKING CONTROL STRATATEGY OF THE MPC WITH THE SPEED CONSTRAINT AND PREVIEW PROCESS

To verify the proposed path tracking control based on model predictive control with adaptive preview characteristics and longitudinal vehicle speed-assisted constraint algorithm, the integrated driving conditions were set for simulation. A circuit condition in Figure 11 (a) was set in the CARSIM, and its starting vehicle speed was set at 72 km/h. The target speed was decelerated for 2 seconds in advance and could only be accelerated on the straight path. The simulation results with Np having the rounding magnitude of 100-1.5(V_{ox} -10) are as follows.

As shown in Figure 11, the lateral error is maintained within [−0.270 m, 0.138 m], the yaw angle error is maintained within [−0.026 rad, 0.029 rad], the lateral acceleration in the curve is maintained at 0.6 g for most of the time, and the largest value is 0.643 g. A few parts exceeded 0.6 g, such as the magnified area in Figure 11 (e), because the longitudinal velocity did not fall below the reference value during the curve.

In addition, Figure 11 (e) shows that the annular road condition has a minimum vehicle speed of 48 km/h under the lateral acceleration constraint of 0.6 g. In the tracking process, only the starting vehicle speed is smaller than the minimum vehicle speed of 48 km/h, and all other vehicles travel at a speed above 48 km/h. Thus, this strategy obviously results in a much lower running time for tracking than with a constant speed of 48 km/h. From the perspective of lateral error and lateral acceleration, the proposed path tracking control strategy of MPC with the speed constraint and preview process achieves the desired performance.

V. CONCLUSION AND FUTURE WORK

A model predictive control is proposed with adaptive preview characteristics and an algorithm of the longitudinal vehicle speed-assisted constraint for the path tracking algorithm. First, an MPC algorithm based on an adaptive preview characteristic of lateral error and target curvature is proposed to improve the tracking performance. Then, this work builds the basic framework of MPC. The lateral acceleration should be constrained in the MPC controller, the vehicle may understeer, and the tracking performance may deteriorate under constraint. Considering this contradiction, a longitudinal vehicle speed control assistant algorithm based on the largest ideal lateral acceleration is proposed to resolve the contradiction and improve vehicle safety and passability. In this study, we found that

(1) The traditional MPC controller generates almost no preview characteristics in the intelligent vehicle path tracking application, but the control strategy of the intelligent vehicle path tracking requires the preview characteristic to improve the tracking performance.

(2) The proposed adaptive preview strategy is suitable for the path tracking algorithm controlled by the MPC controller.

(3) We only consider the vehicle speed constraint that corresponds to the lateral acceleration in the horizontal plane, and the vehicle must be decelerated in advance to satisfy the requirements of no acceleration and deceleration operation in a curve and the corresponding speed of the curve.

(4) The model predictive control with adaptive preview characteristics and an algorithm of the longitudinal vehicle speed-assisted constraint for the path tracking algorithm reduces the running time when the vehicle tracks a specified path with a safe and constant vehicle speed.

However, shortcomings remain in this study: the Np step size is not constant, and the longitudinal speed control could not fully satisfy the constraint. Those issues will be our next research focus.

REFERENCES

[1] A. Bachrach, S. Prentice, R. He, P. Henry, A. S. Huang, M. Krainin, D. Maturana, D. Fox, and N. Roy, "Estimation, planning, and mapping for autonomous flight using an RGB-D camera in GPS-denied environments," *Int. J. Robot. Res.*, vol. 31, no. 11, pp. 1320–1343, Sep. 2012.

[2] C. Zhang, J. Hu, J. Qiu, W. Yang, H. Sun, and Q. Chen, "A novel fuzzy observer-based steering control approach for path tracking in autonomous vehicles," *IEEE Trans. Fuzzy Syst.*, vol. 27, no. 2, pp. 278–290, Feb. 2019.

[3] N. H. Amer, H. Zamzuri, K. Hudha, and Z. A. Kadir, "Modelling and control strategies in path tracking control for autonomous ground vehicles: A review of state of the art and challenges," *J. Intell. Robotic Syst.*, vol. 86, no. 2, pp. 225–254, May 2017.

[4] E. Kim, J. Kim, and M. Sunwoo, "Model predictive control strategy for smooth path tracking of autonomous vehicles with steering actuator dynamics," *Int. J. Automot. Technol.*, vol. 15, no. 7, pp. 1155–1164, Dec. 2014.

[5] S. Xu and H. Peng, "Design, analysis, and experiments of preview path tracking control for autonomous vehicles," *IEEE Trans. Intell. Transp. Syst.*, vol. 21, no. 1, pp. 48–58, Jan. 2020.

[6] Z. Sun, J. Zheng, Z. Man, and H. Wang, "Robust control of a vehicle steer-by-wire system using adaptive sliding mode," *IEEE Trans. Ind. Electron.*, vol. 63, no. 4, pp. 2251–2262, Apr. 2016.
[7] R. Potluri and A. K. Singh, "Path-tracking control of an autonomous 4WS4WD electric vehicle using its natural feedback loops," *IEEE Trans. Control Syst. Technol.*, vol. 23, no. 5, pp. 2053–2062, Sep. 2015.
[8] Y. Xia, F. Pu, S. Li, and Y. Gao, "Lateral path tracking control of autonomous land vehicle based on ADRC and differential flatness," *IEEE Trans. Ind. Electron.*, vol. 63, no. 5, pp. 3091–3099, May 2016.
[9] X. Zhang and X. Zhu, "Autonomous path tracking control of intelligent electric vehicles based on lane detection and optimal preview method," *Expert Syst. Appl.*, vol. 121, pp. 38–48, May 2019.
[10] J. Yang, H. Bao, N. Ma, and Z. Xuan, "An algorithm of curved path tracking with prediction model for autonomous vehicle," in *Proc. 13th Int. Conf. Comput. Intell. Secur. (CIS)*, Dec. 2017, pp. 405–408.
[11] W. Wang, J. Xi, C. Liu, and X. Li, "Human-centered feed-forward control of a vehicle steering system based on a driver's path-following characteristics," *IEEE Trans. Intell. Transp. Syst.*, pp. 1–14, 2016.
[12] W. Wang, J. Xi, C. Liu, and X. Li, "Human-centered feed-forward control of a vehicle steering system based on a driver's path-following characteristics," *IEEE Trans. Intell. Transp. Syst.*, vol. 18, no. 6, pp. 1440–1453, Jun. 2016.
[13] J. Wang, J. Wang, R. Wang, and C. Hu, "A framework of vehicle trajectory replanning in lane exchanging with considerations of driver characteristics," *IEEE Trans. Veh. Technol.*, vol. 66, no. 5, pp. 3583–3596, May 2017.
[14] G. C. Rains, A. G. Faircloth, C. Thai, and R. L. Raper, "Evaluation of a simple pure pursuit path-following algorithm for an autonomous, articulated-steer vehicle," *Appl. Eng. Agricult.*, vol. 30, no. 3, pp. 367–374, 2014.
[15] T. Albin, D. Ritter, N. Liberda, R. Quirynen, and M. Diehl, "In-vehicle realization of nonlinear MPC for gasoline two-stage turbocharging airpath control," *IEEE Trans. Control Syst. Technol.*, vol. 26, no. 5, pp. 1606–1618, Sep. 2018.
[16] L. Dai, Y. Xia, Y. Gao, B. Kouvaritakis, and M. Cannon, "Cooperative distributed stochastic MPC for systems with state estimation and coupled probabilistic constraints," *Automatica*, vol. 61, pp. 89–96, Nov. 2015.
[17] Z. Wang and C.-J. Ong, "Accelerated distributed MPC of linear discrete-time systems with coupled constraints," *IEEE Trans. Autom. Control*, vol. 63, no. 11, pp. 3838–3849, Nov. 2018.
[18] S. Di Cairano, D. Bernardini, A. Bemporad, and I. V. Kolmanovsky, "Stochastic MPC with learning for driver-predictive vehicle control and its application to HEV energy management," *IEEE Trans. Control Syst. Technol.*, vol. 22, no. 3, pp. 1018–1031, May 2014.
[19] H. Guo, J. Liu, D. Cao, H. Chen, R. Yu, and C. Lv, "Dual-envelop-oriented moving horizon path tracking control for fully automated vehicles," *Mechatronics*, vol. 50, pp. 422–433, Apr. 2018.
[20] C. Sun, X. Zhang, L. Xi, and Y. Tian, "Design of a path-tracking steering controller for autonomous vehicles," *Energies*, vol. 11, no. 6, p. 1451, Jun. 2018.
[21] M. Chen and Y. Ren, "MPC based path tracking control for autonomous vehicle with multi-constraints," in *Proc. Int. Conf. Adv. Mech. Syst. (ICAMechS)*, Dec. 2017, pp. 477–482.
[22] G. V. Raffo, G. K. Gomes, J. E. Normey-Rico, C. R. Kelber, and L. B. Becker, "A predictive controller for autonomous vehicle path tracking," *IEEE Trans. Intell. Transp. Syst.*, vol. 10, no. 1, pp. 92–102, Mar. 2009.
[23] J. Ji, A. Khajepour, W. W. Melek, and Y. Huang, "Path planning and tracking for vehicle collision avoidance based on model predictive control with multiconstraints," *IEEE Trans. Veh. Technol.*, vol. 66, no. 2, pp. 952–964, Feb. 2017.
[24] B. Mashadi, M. Mahmoodi-K, A. H. Kakaee, and R. Hosseini, "Vehicle path following control in the presence of driver inputs," *Proc. Inst. Mech. Eng., K, J. Multi-Body Dyn.*, vol. 227, no. 2, pp. 115–132, Jun. 2013.
[25] B. Mashadi, M. Mahmoudi-Kaleybar, P. Ahmadizadeh, and A. Oveisi, "A path-following driver/vehicle model with optimized lateral dynamic controller," *Latin Amer. J. Solids Struct.*, vol. 11, no. 4, pp. 613–630, Aug. 2014.
[26] T. Yuan, K. Krishnan, Q. Chen, J. Breu, T. B. Roth, B. Duraisamy, C. Weiss, M. Maile, and A. Gern, "Object matching for inter-vehicle communication systems—An IMM-based track association approach with sequential multiple hypothesis test," *IEEE Trans. Intell. Transp. Syst.*, vol. 18, no. 12, pp. 3501–3512, Dec. 2017.
[27] C. Sun, X. Zhang, Q. Zhou, and Y. Tian, "A model predictive controller with switched tracking error for autonomous vehicle path tracking," *IEEE Access*, vol. 7, pp. 53103–53114, 2019.
[28] Y. Shen, D. Xiang, X. Wang, L. Jiang, and Y. Wei, "A contact force model considering constant external forces for impact analysis in multibody dynamics," *Multibody Syst. Dyn.*, vol. 44, no. 4, pp. 397–419, Dec. 2018.
[29] S. Aouaouda, M. Chadli, M. Boukhnifer, and H. R. Karimi, "Robust fault tolerant tracking controller design for vehicle dynamics: A descriptor approach," *Mechatronics*, vol. 30, pp. 316–326, Sep. 2015.
[30] M. Park, S. Lee, and W. Han, "Development of steering control system for autonomous vehicle using geometry-based path tracking algorithm," *ETRI J.*, vol. 37, no. 3, pp. 617–625, Jun. 2015.
[31] C. Gámez Serna and Y. Ruichek, "Dynamic speed adaptation for path tracking based on curvature information and speed limits," *Sensors*, vol. 17, no. 6, p. 1383, Jun. 2017.

CHANGHUA DAI received the B.S. degree from Jilin University, Changchun, China, in 2014, where he is currently pursuing the Ph.D. degree with the College of Automotive Engineering.

His research interest includes automotive dynamics simulation and control.

CHANGFU ZONG received the B.S. degree from the Liaoning University of Technology, Jinzhou, China, in 1986, and the M.Eng. and Ph.D. degrees from Jilin University, Changchun, China, in 1994 and 1998, respectively.

He was an Academic Visitor with the University of Cambridge, U.K., in 2005, and a Senior Academic Visitor with the University of California at Berkeley, USA, in 2013. He is currently a Professor with the State Key Laboratory of Automotive Simulation and Control, Jilin University. He has published over 200 articles. His research interests include vehicle control stability, new energy vehicle, intelligent networked automobile control, and autonomous vehicle control.

GUOYING CHEN received the Ph.D. degree from Jilin University, Changchun, Jilin, China, in 2012.

He is currently an Associate Professor with the State Key Laboratory of Automotive Simulation and Control, Jilin University. His research interest includes vehicle dynamics simulation and control.